

Title	Cellulose-based scaffolds for fluorescence lifetime imaging-assisted tissue engineering
Authors	O'Donnell, Neil;Okkelman, Irina A.;Timashev, Peter;Gromovkykh, Tatyana I.;Papkovsky, Dmitri B.;Dmitriev, Ruslan I.
Publication date	2018-09-25
Original Citation	O'Donnell, N., Okkelman, I. A., Timashev, P., Gromovkykh, T. I., Papkovsky, D. B. and Dmitriev, R. I. (2018) 'Cellulose-based scaffolds for fluorescence lifetime imaging-assisted tissue engineering', Acta Biomaterialia, 80, pp. 85-96. doi:10.1016/j.actbio.2018.09.034
Type of publication	Article (peer-reviewed)
Link to publisher's version	10.1016/j.actbio.2018.09.034
Rights	© 2018, Elsevier Ltd. All rights reserved. This manuscript version is made available under the CC-BY-NC-ND 4.0 license. - https://creativecommons.org/licenses/by-nc-nd/4.0/
Download date	2023-05-04 21:13:23
Item downloaded from	http://hdl.handle.net/10468/7080

Please cite this article as:

O'Donnell N, Okkelman IA, Timashev P, Gromovych TI, Papkovsky DB, Dmitriev RI: **Cellulose-based scaffolds for fluorescence lifetime imaging-assisted tissue engineering**. *Acta Biomaterialia* 2018, **80**:85-96.

Final manuscript version is available at:

<https://www.sciencedirect.com/science/article/pii/S1742706118305634>

Cellulose-based scaffolds for fluorescence lifetime imaging-assisted tissue engineering

Neil O'Donnell^{1*}, Irina A. Okkelman^{1*}, Peter Timashev^{2,3}, Tatyana I. Gromovych⁴, Dmitri B. Papkovsky¹, Ruslan I. Dmitriev^{1,2Δ}

¹ School of Biochemistry and Cell Biology, University College Cork, Cork, Ireland.

² Institute for Regenerative Medicine, I.M. Sechenov First Moscow State University, Moscow, Russian Federation

³ Institute of Photonic Technologies, Research Center 'Crystallography and Photonics, Russian Academy of Sciences, Moscow, Russian Federation

⁴ Department of Biotechnology, I.M. Sechenov First Moscow State University, Moscow, Russian Federation

*These authors contributed equally to this work;

ΔAddress for correspondence: Cavanagh Pharmacy Building, University College Cork, College Road, Cork, Ireland. Phone: 0214901339. E-mail: r.dmitriev@ucc.ie

Abstract

Quantitative microscopy of pH and metabolite gradients is among the challenges for production of scaffold-grown organoids and multi-cellular aggregates. Here, we utilized the cellulose-binding domain (CBD) of *C. fimi* CenA protein for design of biosensor scaffolds allowing measurement of pH and Ca²⁺ gradients in fluorescence intensity and lifetime imaging (FLIM) detection modes. By fusing CBD to pH-sensitive enhanced cyan fluorescent protein (CBD-ECFP) we achieved efficient labeling of cellulose-based scaffolds based on nanofibrillar, bacterial cellulose and decellularized plant materials. CBD-ECFP bound to the cellulose matrices demonstrated pH sensitivity comparable to untagged ECFP (1.9-2.3 ns for pH 6-8), making it compatible with FLIM-based analysis of extracellular pH. Using 3D culture of human colon cancer cells (HCT116) and adult stem cell-derived mouse intestinal organoids, we evaluated the utility of the produced biosensor scaffold. CBD-ECFP was sensitive to increases in extracellular acidification, showing drop in 0.2-0.4 pH units in response to membrane depolarization by the protonophore FCCP. With the intestinal organoid model, we demonstrated multi-parametric imaging by combining extracellular acidification (FLIM) with phosphorescent probe-based monitoring of cell oxygenation. The described labeling strategy allows for the design of extracellular pH-sensitive scaffolds for multi-parametric FLIM assays and their use in engineered live cancer and stem cell-derived tissues. Collectively, this research can help achieving the controlled bio-fabrication of 3D tissue models with known metabolic characteristics.

Keywords

Biomaterials; Biosensor; FLIM; Live cell imaging; Organoid; Scaffold

1. Introduction

Being the most abundant organic polymer on our planet, cellulose is employed in tissue engineering, photonics, biosensing and biomaterials research [1]. In tissue engineering applications, cellulose displays features of an ideal scaffold material for cell and tissue growth, being biocompatible, biodegradable and cost-effective. Available in form of cellulose nanocrystals, nanofibrillar and bacterial cellulose and complemented by the set of related carbohydrate-based polymers, cellulose is already used as the scaffolding and 3D printed material [2-5] for cartilage tissue regeneration [6], bone tissue [7], differentiating endothelial cells [8] and wound repair [9]. Diverse approaches allow modifying the cellulose-derived scaffolds to improve the cell adhesion, biocompatibility and provide the modular scaffold architecture. These include: (a) chemical modification with polyethyleneglycole, thiols and other oligo- and polymers [3]; (b) use of proteins with cellulose-binding domains [4, 10] and (c) biosynthetic modification [11]. Recently, the concept of using decellularized plant materials (leaves, petioles) was proposed for animal tissue engineering and production of so-called 'plantimals' [12, 13]. Providing broad choice of physical characteristics (porosity, tensile strength) and presence of vascular network, highly compatible with further modification with extracellular matrix and other molecules [13], decellularized plant materials open new perspectives in animal tissue engineering.

With the broad variety of already available scaffold materials, modern tissue engineering switches its focus to the functional analysis of essential biomarkers and the use of scaffolds *to direct* the development of engineered 3D tissue models and organoids [14-16]. In particular, stem cell niche maintained in 3D culture is affected by the external and internal cues including physical, chemical and biological factors, such as pH, Ca^{2+} , material stiffness, extracellular matrix and others [17]. Many of these factors are equally important for tissue engineering in cancer research [18] and can be modulated using the scaffolds.

Extracellular acidification is one of the key biomarkers in cancerous and normal non-transformed tissues [19]. Being indicative for the glycolytic flux, it can be directly used for analysis of cell energy budget, assessing the balance of oxidative phosphorylation, glycolysis and other cell energy production pathways [20]. The role of extracellular pH has been already appreciated in bone tissue engineering [21], drug and growth factor delivery [22] and (re)modeling of extracellular matrix [23]. Regulation of extracellular Ca^{2+} is also of utter importance for most of the tissues in the body, especially for signaling at the interface of the extracellular matrix, e.g. by stimulating differentiation of goblet cells in gastrointestinal tract [24] and affecting cell bioenergetics in neurosecretory cells [25].

While monitoring of extracellular pH and Ca^{2+} was never realized in tissue-engineered constructs, the variety of small molecule dyes, nanoparticles and fluorescent proteins [26] make it possible. Some of these sensor probes allow for quantitative measurements, by means of ratiometric intensity-based detection and fluorescence lifetime imaging microscopy (FLIM) [27]. The latter method is now preferred for quantitative measurements allowing for intensity-insensitive calibration reporting the absolute values of measured analyte and is also useful for multiparametric microscopy assays [28-30]. FLIM-based pH sensing can be performed using a number of proteins, such as enhanced cyan fluorescent protein (ECFP) [31], pHRed [32], some small molecule dyes [33, 34] and pH-sensitive nanoparticles [35].

The inventory of Ca^{2+} -sensing probes is also comprehensive, ranging from dyes to advanced fluorescent proteins, with some of them being sensitive in FLIM [36-39].

In light of this, it is interesting to see if the cellulose scaffolds for tissue engineering can be further modified to become biosensors for extracellular pH and Ca^{2+} , similarly to the phosphorescent hybrid biosensing scaffolds [40-42]. While modification of cellulose has been already suggested for biosensing with nanocrystals [43], FRET-based enzyme constructs in wound healing and with gold nanoparticles immobilized via antibody [44], only few published studies are practical for imaging-assisted tissue engineering [45-47].

In order to find a simple and efficient way of modifying cellulose with biosensor proteins, we looked at the cellulose-binding domain (CBD), known for decades and initially described as a tag for affinity purification of proteins [48, 49]. Nearly 200 protein domains vary in the structure, size (4-20 kDa) and specificity towards binding cellulose [50]. Association with cellulose can be reversed by the presence of denaturants or competitive elution with cellobiose. In particular, *Cellulomonas fimi* CenA protein fragment [51], was successfully used as affinity tag in bacterial, yeast and mammalian expression systems, maintaining solubility and folding of fused proteins [50]. Surprisingly, this and related proteins tags, allowing for specific and affinity modification of cellulose-based and related scaffolds, were rarely used in tissue engineering [4].

Here, we investigated the feasibility of combining the cellulose-binding domain with fluorescent protein biosensor. Resulting chimeric protein can bind the cellulose and produce the hybrid pH or Ca^{2+} -sensing matrices, useful as tissue engineering scaffolds. With the help of designed biosensors and FLIM method, we demonstrated quantitative pH sensing in the engineered cellulose-based 3D culture of cancer cells and the intestinal organoid model and tested it in multi-parametric analysis of cell oxygenation.

2. Materials and methods

2.1. Materials and chemicals

Antarctic Phosphatase, restriction enzymes *Bam* HI, *Hin* dIII-HF, *Kpn* I, *Sma* I, T4 DNA polymerase were from New England Biolabs (Brennan & Co, Dublin, Ireland), T4 DNA Ligase, 2X PCR buffer, Wizard MiniPreps Plasmid DNA purification and SV Gel Clean-up kits were from Promega (MyBio, Ireland).

Plasmid DNA GCaMP2-pRSET B (Amp^R) [52] was provided by Prof. H. Sondermann (Cornell University, USA). Plasmid DNA encoding ECFP in pProEx HTA (Amp^R) [31] was provided by Prof. M. Erard (Universite Paris Sud, France).

O_2 -sensitive phosphorescent probe Pt-Glc was synthesized as described before [53, 54]. pH-Extra phosphorescent probe was from Luxcel Biosciences (Little Island, Cork), '15 μ -slide III' 3D perfusion chamber slides were from Ibidi GmbH (Martinsried, Germany). GrowDex scaffolds were from UPM Biochemicals (Helsinki, Finland).

Fresh plant materials (spinach leaves *Spinacia oleracea*, celery 'stems' petioles *Apium graveolens*) were purchased from local vendors (Lidl and Marks & Spencer, Cork, Ireland).

Bicinchoninic acid (BCA) protein assay kit was from Thermofisher (Dublin, Ireland). Lysozyme, Tetramethylrhodamine methyl ester (TMRM), LB broth, protease inhibitor

cocktail, CellLytic B and all the other reagents were from Sigma-Aldrich (Dublin, Ireland).

The protein 3D structures available from Protein DataBank (rcsb.org) were viewed and exported using NGL software [55]: GCaMP2 Ca^{2+} -saturated monomer (3EK4) [56], ECFP (2WSN)[57] and *C. fimi* cellulose binding domain (1EXG)[58].

2.2. Cloning of CBD-ECFP and CBD-GCaMP2. Codon-optimized sequence encoding N-terminal CBD-CenA fragment (Ala³²-Thr¹³⁷, see Supplementary Info 1), with introduced flanking *Bam* HI, *Kpn* I and *Sma* I restriction digest sites, commercially synthesized by Genscript (Piscataway, NJ, USA) and supplied in pUC-57 plasmid, was subcloned in frame with the human ferritin sequence in pQE-30 plasmid, which was subsequently deleted to produce CBD Δ (FTN) plasmid DNA, by digesting with *Sma* I and *Hin* dIII enzymes, followed by treatment with T4 DNA polymerase and self-ligation (Supplementary Info 1). ECFP and GCaMP2 coding sequences, synthesized by Genscript and supplied in pUC-57 plasmid, were used as templates for cloning of constructs encoding fusions with CBD: they were amplified using polymerase chain reaction (PCR) (15 cycles) with plasmid DNA as template and primers introducing *Kpn* I restriction site, then cloned in CBD Δ (FTN) plasmid DNA, digested with *Kpn* I, pre-treated with Antarctic Phosphatase, ligated and transformed in *E. coli* SG13009 (Qiagen) cells. Coding sequences from resulting plasmids are presented in Supplementary Info 1, Table S1. CBD-fusions were produced with and without GTGGSGG peptide linker between CBD and fluorescent protein. All the produced expression constructs were verified by sequencing (GATC Biotech AG).

2.3. Cellulose scaffolds

Bacterial cellulose was produced by *Gluconacetobacter hansenii* GH-1/2008 (VKPM B-10547). Inoculation material was cultured in the modified Hestrin-Schramm medium (g/L: sucrose – 20, peptone – 5, yeast extract – 5, Na_2HPO_4 – 2.7, citric acid monohydrate – 1.15) [59] at 30°C for 3 days on a rotary shaker. The cellulose production was carried out in the same medium at 26±2°C (150 rpm, 10 days). Next, the medium was removed and cellulose spheres were subsequently washed with distilled water (three times, 24 h each) and with 5% sodium dodecyl sulfate (SDS) (once, 24 h). Finally, the cellulose was rinsed with distilled water and sterilized by immersing in 70% ethanol. Micromechanical properties were measured via a Piuma nanoindenter (Optics11, Netherlands) in distilled water at room temperature using a cantilever with spring constant 0.052 N/m and radius of curvature 9 μm ; the indentation depth was 5 μm . Surface roughness was assessed using a 3D microscope HRM-330T-U3A (Huvitz, South Korea).

Decellularization (DC) of plant tissues was performed accordingly to the method of Fontana et al [13] with modifications: spinach leaves (cut with 5 mm diameter puncher) or celery stems (petioles cut in ~1 mm thick sections) were pre-treated with hexane, washed with phosphate buffered saline, PBS (137 mM NaCl, 2.7 mM NaCl, 10 mM Na_2HPO_4 , 1.8 mM KH_2PO_4 , pH 7.4) and incubated consequently in 10% SDS (4 days), mixture of 10% sodium hypochlorite / 0.1% Triton X100 (48 h) and deionized water (48 h) with gentle rocking at room temp. Decellularized tissues were stored at 4°C for 2 weeks in the presence of sodium azide (0.05%) or were sterilized

by immersing in 70% ethanol and sequential washing in sterile Hanks' Balanced Salt Solution (Sigma H9269) for cell-based experiments.

For imaging on an upright microscope, GrowDex and decellularized tissues were embedded in Matrigel (50% scaffold: 50% Matrigel by volume)

2.4. Bacterial production and purification of proteins. Labeling of scaffolds

CBD-ECFP and CBD-GCaMP2 proteins were produced in *E. coli* SG13009 as described previously [60], with minor modifications: after reaching $OD_{600} = 0.3-0.4$, bacteria grown in the presence of ampicillin (100 $\mu\text{g/ml}$) and kanamycin (25 $\mu\text{g/ml}$) were induced with 0.25 mM isopropyl- β -D-thiogalactopyranoside (IPTG) (room temp., 18 h), harvested and stored as pellets at -80°C . For protein extraction, they were defrosted on ice and lysed in modified 'MiniSOG' buffer (0.2 M NaCl, 30 mM NaH_2PO_4 , 2 mM Tris-HCl, pH 8.3, 0.25 mg/ml lysozyme, 1X CellLytic B and protease inhibitor cocktail (Sigma P2714)) on ice over 30 min, passed through 22 $\frac{1}{2}$ G syringe needle (5 times) and cleared by centrifugation (14,000g, 15 min). Cleared lysates were purified on Ni^{2+} -NTA resin essentially as described previously [60]. Purified proteins were dialyzed against phosphate-buffered saline (PBS) and stored at 4°C (2-3 weeks). For sterilization, proteins were filtered through Spin-X 0.22 μm centrifuge filters (Corning Costar). Purity of proteins was confirmed by SDS-PAGE (typical yields ~ 6 mg/L culture, folding rate (assessed by UV-Visible spectrophotometry) of $\sim 55-70$ %).

2.5. Spectral, plate reader and solution-based fluorescence lifetime measurements

Absorption spectra were measured on an 8453 diode array spectrophotometer (Agilent), fluorescence spectra were measured on LS50B (PerkinElmer) spectrometer in PBS, pH 7.4, as described previously [61]. Solution-based fluorescence lifetime measurements were carried out on Fluorolog-3 (Horiba) Spectrofluorometer at range of pH values using buffer solutions (adapted from [35]) based on 135 mM KCl, 2 mM CaCl_2 , 1 mM MgCl_2 , 20 mM Sucrose and 10% fetal bovine serum (FBS) and supplemented with either 10 mM MES (pH 5.8-6), 10 mM MOPS (pH 6.4-7.2), or 10 mM HEPES-Na (pH 7.6-8). Extracellular acidification rates (ECA) were measured on Victor2 TR-F microplate reader and normalized for total protein content as described before [62].

2.6. Cell and organoid culture

Human colon cancer HCT116 wild-type (WT) and $\text{SCO}_2^{-/-}$ cells were grown in McCoy 5A medium supplemented with 10% fetal bovine serum (FBS) essentially as described before [63]. For microscopy, 150,000 to 300,000 cells were mixed with 0.5% GrowDex and embedded in 50 μL Matrigel in the center of 35 mm TC Petri dish, grown for 2-3 days and analyzed in Phenol Red-free DMEM supplemented with 10 mM glucose, 1 mM sodium pyruvate, 2 mM l-glutamine, pH 7.4. For ECA assay, cells were seeded on collagen IV pre-coated 96-well plate (10,000-100,000 per well) and grown for 2 days before the analysis.

Primary mouse intestinal organoids from adult C57Bl6/J mice (Harlan, UK) were produced essentially as described before [64, 65]. All procedures with animals were performed under the license issued by the Department of Health and Children

(Ireland) and in accordance with the Directive 2010/63/EU adopted by the European Parliament and the Council of the European Union. Briefly, crypts isolated from proximal half of small intestinal tissue were seeded in Matrigel matrix (500 crypts per 50 μ l of gel in 24-well plate) and grown in organoid Growth medium (Advanced DMEM F12 supplemented with 2 mM GlutaMax, 10 mM HEPES-Na, pH 7.2, 1% N2 media supplement (Invitrogen), 2% B27 media supplement (Invitrogen), 1.25 mM N-acetylcysteine, 100 ng/ml mouse recombinant noggin (Peprotech, USA), 1 μ g/ml human recombinant R-spondin 1 (Peprotech, USA), 50 ng/ml mouse recombinant epithelial growth factor (Peprotech, USA) and 1% penicillin-streptomycin). Organoid culture was passaged (1:5) once a week using mechanical disruption of organoids in Matrigel, followed up by its depolymerization in 'Organoid Harvesting Solution' (Cultrex, USA) according to manufacturer's protocol. Intact organoids for seeding in decellularized scaffolds were obtained similarly, avoiding the mechanical disruption stage. Seeding in decellularized celery was performed by mixing primary crypts or dissociated intact organoids with fresh Matrigel (200 μ l total volume) and spreading on the surface of celery, incubation on ice (5 min), followed up by solidification at 37°C. Organoids were then cultured in decellularized celery with Matrigel for 3-10 days prior to the imaging. Similarly, organoids were seeded in GrowDex using mixing with ice-cold Matrigel (2:1 by volume) and drop-solidified in 20 μ l volume on standard pre-warmed 35 mm TC dishes (Sarstedt). To label the produced celery- and GrowDex-based scaffold cultures CBD-ECFP was added (5 μ M, 18 h), followed up by staining with O₂ probe Pt-Glc (2 μ M, 90 min). Measurements were performed in Phenol Red-free DMEM supplemented with 10 mM glucose, 1 mM sodium pyruvate, 2 mM GlutaMax, pH 7.4.

2.7. Microscopy

Optimization of staining with CBD-tagged proteins, stability and assessment of cell growth were performed on Axiovert 200 inverted fluorescence PLIM microscope [62] equipped with T/O₂ control (T=37°C) and LED excitation sources (390, 470 and 590 nm). CBD-tagged proteins were excited using 470 nm LED with emission collected at 510-560 nm, using 10x/0.3 or oil-immersion 40x/1.3 Plan Neofluar objectives. Hoechst 33342-stained cells were excited using 390 nm LED with emission collected with DAPI filter.

FLIM was performed on Axio Examiner Z1 upright laser-scanning FLIM-PLIM microscope [63] equipped with 5x/0.25 Fluor, 20x/1.0 W-Plan and 63x/1.0 W-Plan Apochromat dipping objectives, integrated T and Z-axis controls, DCS-120 confocal TCSPC scanner, photon counting detectors and SPCImage software (Becker & Hickl GmbH). Pt-Glc and TMRM probes were excited using 405 nm BDL-SMNI pulsed diode laser with emission collected at 635-675 nm (Pt-Glc) or at 565-605 nm (TMRM). CBD-GCaMP2 was excited using 488 nm BDL-SMNI pulsed diode laser (emission collected at 512-536 nm), CBD-ECFP was excited using 447 nm BDL-SMT pulsed diode laser (emission collected at 512-536 nm). pH calibration of fluorescence lifetimes of CBD-ECFP was carried out with GrowDex-stained scaffolds in buffer solutions based on 135 mM KCl, 2 mM CaCl₂, 1 mM MgCl₂, 20 mM Sucrose and 10% fetal bovine serum (FBS) adapted from [35] and supplemented with either 10 mM MES (pH 5.8-6), 10 mM MOPS (pH 6.4-7.2), or 10 mM HEPES (pH 7.6-8). Cell stimulations were carried out in Phenol Red-free DMEM as above, using

Please cite this article as:

O'Donnell N, Okkelman IA, Timashev P, Gromovkykh TI, Papkovsky DB, Dmitriev RI: **Cellulose-based scaffolds for fluorescence lifetime imaging-assisted tissue engineering**. *Acta Biomaterialia* 2018, **80**:85-96.

Final manuscript version is available at:

<https://www.sciencedirect.com/science/article/pii/S1742706118305634>

1 μ M Carbonyl cyanide-4-(trifluoromethoxy)phenylhydrazone (FCCP) and 10 μ M oligomycin or with equal amounts of DMSO (mock).

2.8. Data assessment

Plate reader data represent averaged values with standard deviation shown as error bars, as described previously [62]. Fluorescence intensity images exported from widefield (ImSpector Pro software, LaVision) or TCSPC-FLIM (SPCImage software, Becker & Hickl) microscopes were used as is, or (where indicated) additionally processed for deconvolution ('express deconvolution' option) and assembled as 3D stacks in SVI Huygens Pro 17.0 software (Scientific Volume Imaging BV, Netherlands). For quantification of scaffold staining efficiency, stability and cell growth the fluorescence intensity images were analyzed in ImageJ software (Fiji.sc). Cell nuclei stained with Hoechst 33342 were counted in ImageJ software using 3D object counter plugin.

For pH calibration, the fluorescence lifetime distribution histograms (produced in SPCImage with optimised fitting function, three independent replicates per each pH point) were exported in Origin 6.0 software (Microcal Inc., USA), fit with Cauchy-Lorentz distribution function to identify mean values and fitted for corresponding pH values using Sigmoid function in Origin 6.0. The following relationship was obtained for CBD-ECFP (447 nm exc.):

$$\tau = \frac{2133}{1 + e^{-1.42 \cdot (pH - 4.89)}} \quad (1.1), \text{ where } \tau \text{ is in ps.}$$

For conversion of measured fluorescence lifetime values in pH, a simplified polynomial relationship was used:

$$pH = 16.48 - 0.0141 \cdot \tau + 4.56 \cdot 10^{-6} \cdot \tau^2 \quad (1.2), \text{ where } \tau \text{ is in ps.}$$

O₂ calibration equation for Pt-Glc in intestinal organoids was used as described before [65]. Fluorescence lifetime data were routinely processed in Excel 2007 (Microsoft) software and combined in Adobe Illustrator CS2 (Adobe).

2.9. Statistical methods

The microscopy experiments were performed in triplicate with the data presented as mean values from 8-9 independently chosen regions of interest (ROI) and where appropriate were tested for statistical significance using independent *t*-test. The fluorescence lifetime decays were fit directly in SPCImage software (Becker & Hickl) using tail-enhanced mono-exponential or double-exponential fitting functions to achieve $\chi^2 < 1.5$. Fitted fluorescence and phosphorescence lifetime data from selected ROIs (pixel matrices with $N > 200$ for Fig. 4G and $N > 90$ data points for Figure 5G) were tested for statistical significance (independent *t*-test for two populations, with significance levels $p < 0.05$ considered to be significant).

3. Results and discussion

3.1. Design and choice of the proteins

In order to design the efficient cellulose-binding biosensor, we selected *Cellulomonas fimi* CenA fragment Ala³²-Thr¹³⁷ (further referred as 'cellulose-binding domain',

CBD), which has relatively small size (113 a.a., 11.5 kD), high solubility and expression yields and folding in bacteria [50, 51, 66]. Literature search identified a number of prospective FLIM protein-based biosensors, which can be attached C-terminally to the CBD. Thus, for pH we chose ECFP, which possess strong pH-sensitivity of fluorescence lifetime (excited by blue light and emitting in blue-green) and previously demonstrated in intracellular pH-FLIM [31]. For Ca^{2+} biosensor we used GCaMP2 protein showing structural changes upon binding Ca^{2+} , which can potentially affect its fluorescence lifetime [67, 68]. It is also compatible with green laser light (488 nm), which is convenient for tissue culture-based measurements. The biosensor proteins were initially cloned without linker, to produce C-terminal fusion with CBD. However we found that incorporation of short Gly-rich linker GlyThrGlyGlySerGlyGly significantly improved the folding rate of produced proteins (Experimental procedures 2.2, Fig. 1). For simplicity, Gly-linker containing proteins are further referred as CBD-ECFP and CBD-GCaMP2. The designed proteins are schematically shown in Fig. 1A, based on their available high-resolution 3D structures (Experimental procedures, section 2.1).

Using metal chelate affinity chromatography, we efficiently purified produced proteins, without noticeable non-specific binding of CBD to the Ni^{2+} -NTA agarose beads (proteins were eluted using imidazole). Purified proteins (Fig. 1) showed yields of ~6 mg/ L culture, with folding rates of 55-70% (assessed by UV-Visible spectroscopy). Both CBD-ECFP and CBD-GCaMP2 demonstrated sensing properties in solution, in fluorescence intensity mode (Fig. 1 C, E): approximately twofold response of intensity was noted for pH probe and ~1.25 fold for Ca^{2+} probe (aggregation was noted with higher concentrations of Ca^{2+}). This is very comparable to the untagged proteins, suggesting minimal or no negative effects of fusion with CBD. We also measured fluorescence lifetimes in solution for ECFP and CBD-ECFP (Fig. S1), observing magnitude of response from 1.9 ns (pH 6) to 2.3 ns (pH 8), in agreement with the literature data [31].

Thus, we successfully produced recombinant CBD-tagged fusions of pH- and Ca^{2+} - sensitive fluorescent proteins, which demonstrated expected bright fluorescence in solution.

Please cite this article as:

O'Donnell N, Okkelman IA, Timashev P, Gromovych TI, Papkovsky DB, Dmitriev RI: **Cellulose-based scaffolds for fluorescence lifetime imaging-assisted tissue engineering**. *Acta Biomaterialia* 2018, **80**:85-96.

Final manuscript version is available at:

<https://www.sciencedirect.com/science/article/pii/S1742706118305634>

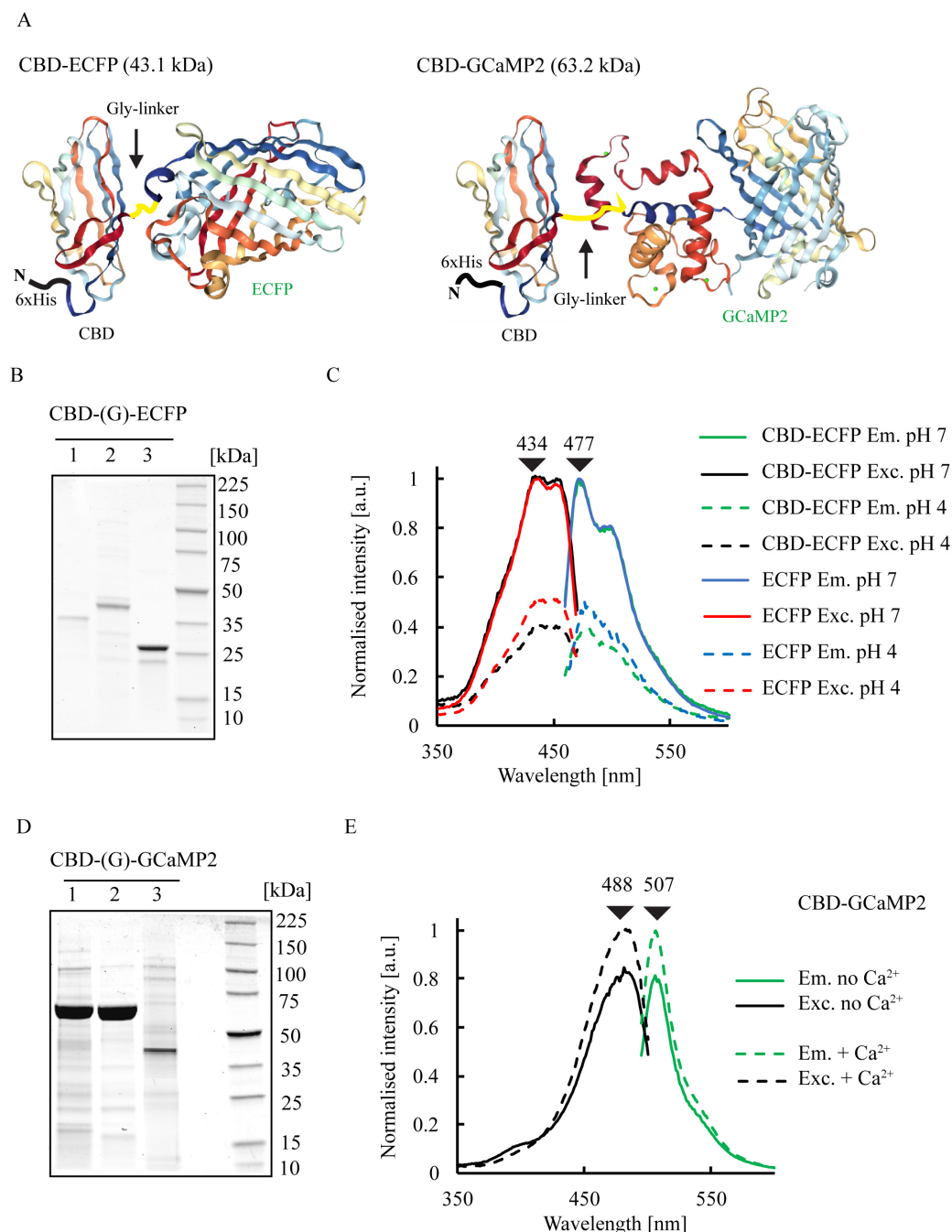


Figure 1. Design and evaluation of CBD-tagged biosensors. A: Schematic representation of designed proteins. N-terminal 6xHis sequences are shown in black, Gly-rich linker regions are shown in yellow. Note that GCaMP2 is shown in Ca^{2+} -saturated form. B: SDS-PAGE analysis of purified CBD-ECFP without Gly-linker (1), with Gly-linker (2) and ECFP (3). C: Normalized fluorescence spectra of purified CBD-ECFP and ECFP in solution at different pH. D: SDS-PAGE analysis of purified CBD-GCaMP2 without Gly-linker (1), with Gly-linker (2) and GCaMP2 (3). E: Normalized fluorescence spectra of purified CBD-GCaMP2 in Ca^{2+} -free form and after adding 1 mM CaCl_2 .

3.2. Staining of cellulose-based materials and their sensing properties

To study the interaction of purified CBD-ECFP and CBD-GCaMP2 biosensors with cellulose we chose a number of different matrices. First, we used commercially available nanofibrillar cellulose known as GrowDex. When we simply incubated purified CBD-ECFP with this matrix (15 min, room temp., one wash step), we observed efficient staining, well distinguishable from background signals at concentrations $> 2 \mu\text{M}$ (0.5% GrowDex) (Fig. 2A). Optical sectioning using confocal microscopy confirmed efficient three-dimensional in-depth staining of GrowDex with CBD-ECFP (Fig. 2B). Staining of GrowDex was concentration-dependent and reached saturation at $\sim 10 \mu\text{M}$ concentration (Fig. 2C). We found that CBD-ECFP staining of GrowDex was stable, decreasing its fluorescence after 10 days of storage in solution at 4°C only by 20% (Fig. 2D). In contrast, we did not see the significant degree of GrowDex staining with untagged ECFP, as observed from background signals (Fig. S2). Similar data were observed with CBD-GCaMP2, which possessed comparable kinetics of staining and storage stability (Figs. S2-S3).

Next, we tested a number of different cellulose-based scaffolds suitable for 3D cell culture: bacterial cellulose and decellularized materials (DC) produced from plants.

The bacterial cellulose samples produced using conventional method [59] (Fig. S4) were cut in small pieces ($\sim 2 \times 5 \text{ mm}$) for the experiments. Bacterial cellulose also showed similar staining efficacy with CBD-ECFP as the GrowDex (Fig. 2D) although it provided lower quality images on a widefield fluorescence microscope. 3D reconstruction of stained bacterial cellulose showed highest brightness for the periphery / surface regions of $\sim 20\text{-}30 \mu\text{m}$ depth (Fig. 2E). This can be explained by the limited light penetration due to more solid and less transparent nature of this material, especially with blue-green emitting ECFP protein.

The decellularized (DC) materials were recently proposed as an alternative scaffold material, sourced from widely available plants already having good porosity and well-developed vascular system. We tested two different plant-based materials, produced from spinach leaf and celery stems. Using fluorescence microscopy, we controlled the decellularization process (Fig. S5, 2G): it was evident that after decellularization procedure, plant materials became optically clear and non-fluorescent in blue-green spectral channels and retained their 3D architecture. The incubation with CBD-ECFP (12-16 h) in phosphate buffered saline, pH 7.4 (PBS) or culture medium allowed efficient and specific staining, especially in case of celery stems having high porosity (Fig. S5-S6). Somewhat slower staining procedure than with GrowDex and bacterial cellulose can be explained by a more limited diffusion of proteins and biomolecules within these matrices. Overall, both spinach and celery DC materials labeled with CBD-ECFP remained stable upon 7-14 days ensuring their suitability for biosensing applications.

Thus, we observed efficient staining of various cellulose-based scaffold materials with CBD-ECFP and CBD-GCaMP2 biosensors. With GrowDex and DC celery we achieved the highest staining efficacy and specificity. This can be explained by patch-like structure of GrowDex (i.e. scaffold represents floating agglomerates of nanofibrillar cellulose) and high porosity of DC celery stems. Both of these materials are attractive for cell-based applications.

Please cite this article as:

O'Donnell N, Okkelman IA, Timashev P, Gromovych TI, Papkovsky DB, Dmitriev RI: **Cellulose-based scaffolds for fluorescence lifetime imaging-assisted tissue engineering**. *Acta Biomaterialia* 2018, **80**:85-96.

Final manuscript version is available at:

<https://www.sciencedirect.com/science/article/pii/S1742706118305634>

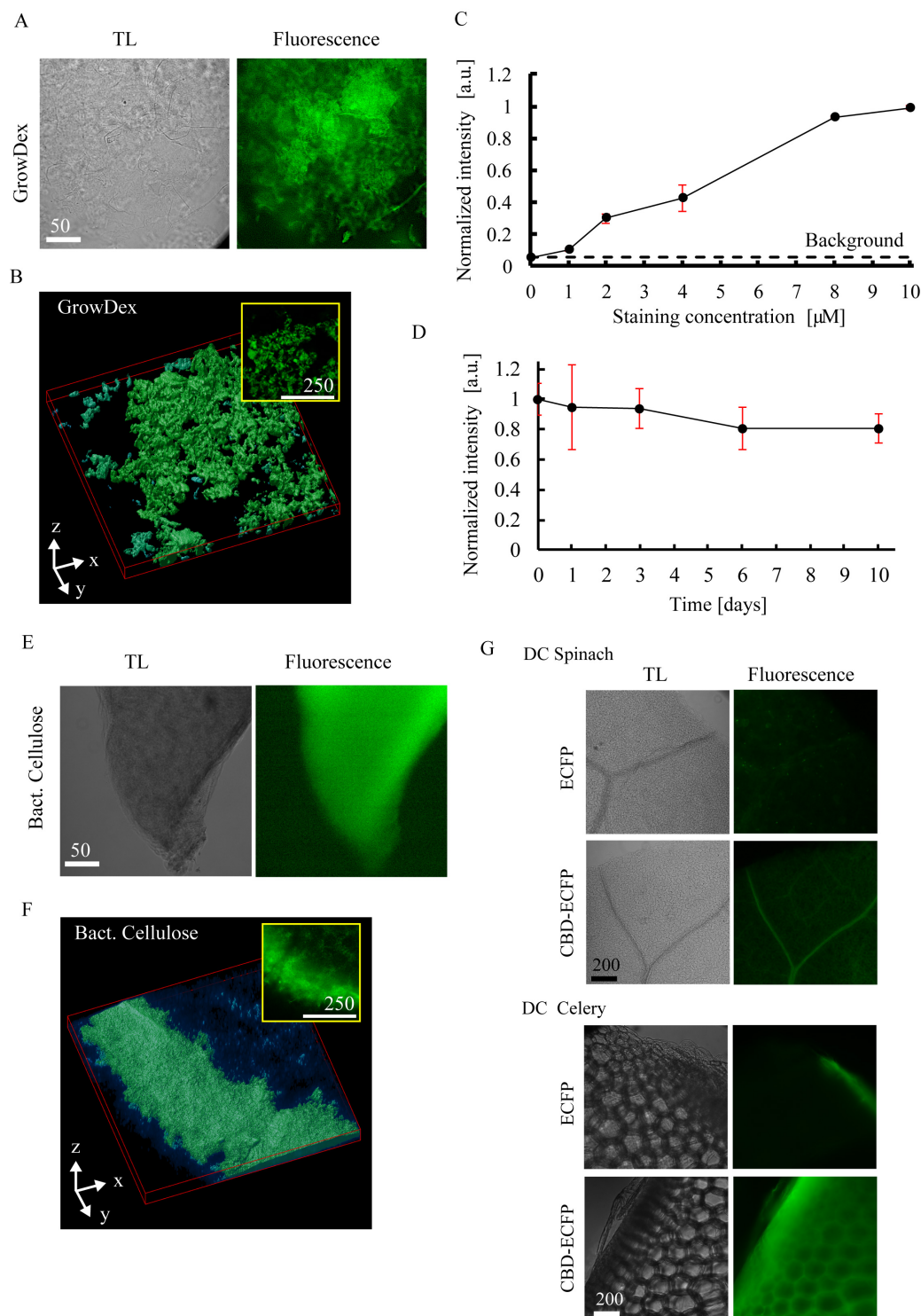


Figure 2. Staining of cellulose scaffolds with CBD-ECFP. A: transmission light (TL) and fluorescence (470 nm exc., 510-650 nm em.) microscopy images of GrowDex stained with CBD-ECFP (5 μ M, 15 min). B: 3D reconstructions (45 μ m Z stack) of CBD-ECFP-stained GrowDex scaffold (447 nm exc., 512-536 nm em.). Inserts show the scale and the top section. C: Dependence of the GrowDex fluorescence from CBD-ECFP staining concentration (15 min staining time), measured by fluorescence microscopy. The data were normalized to the maximal background-corrected fluorescence signals. D: Stability of CBD-ECFP-stained

Please cite this article as:

O'Donnell N, Okkelman IA, Timashev P, Gromovskiy TI, Papkovsky DB, Dmitriev RI: **Cellulose-based scaffolds for fluorescence lifetime imaging-assisted tissue engineering**. *Acta Biomaterialia* 2018, **80**:85-96.

Final manuscript version is available at:

<https://www.sciencedirect.com/science/article/pii/S1742706118305634>

GrowDex scaffold fluorescence measured by microscopy of the sample (stained with 10 μ M, 15 min) over 10 days. The data were normalized to the initial background-corrected fluorescence. E: transmission light (TL) and fluorescence microscopy images of bacterial cellulose stained with CBD-ECFP (5 μ M, 15 min). F: 3D reconstructions (45 μ m Z stack) of CBD-ECFP-stained bacterial cellulose. G: transmission light and fluorescence microscopy images of DC spinach and celery tissues stained with CBD-ECFP (5 μ M, 16 h). Scale bar is in μ m.

Using GrowDex scaffold stained with CBD-ECFP, we performed FLIM experiments in buffer solutions with different pH. We routinely used 'traditional' for calibration of intracellular pH sensors KCl-containing buffer (Experimental procedures, section 2.5), since the buffer with NaCl showed no effect on ECFP fluorescence (not shown). The fluorescence decays of ECFP fitted using double-exponential function showed pH-sensitive changes, evident by analysis of distribution histograms or FLIM images in color-coded scale (Fig. 3A-C). By exposing CBD-ECFP scaffolds to pH across the physiological range we performed the calibration. As expected, ECFP demonstrated pK_a values close to the literature data (~4.9), which are acidic but still useful for cellular pH measurements [31]. In agreement with this, calibration demonstrated highest sensitivity of the protein in range of pH 5.5-7, although significant changes were observed only for range of pH 6-7 (Fig. 3D). Thus, CBD-ECFP protein can be potentially used for quantitative FLIM-based pH sensing although it does not possess ideal sensitivity.

Similarly, we evaluated CBD-GCaMP2 protein as FLIM biosensor. GCaMP2 and its modifications were successfully used in *in vivo* intensity-based measurements [56] and we wondered if this protein can show changes in fluorescence lifetime. We exposed the matrix to various concentrations of Ca²⁺ but did not observe meaningful responses in fluorescence lifetime over 0-5 mM concentrations (Fig. 3E) Thus, in our hands GCaMP2 did not show sensitivity to Ca²⁺ in fluorescence lifetime readout.

Collectively, both designed fluorescent proteins demonstrated strong ability to label cellulose scaffolds and are potentially useful as biosensing reagents. However, only CBD-ECFP displayed plausible pH-sensing properties in FLIM, beneficial for analysis of highly glycolytic cells and tissues, which can acidify the extracellular environment. This data also shows that potentially any other prospective biosensor can be cloned as a fusion with CBD tag to produce the biosensor cellulose matrices.

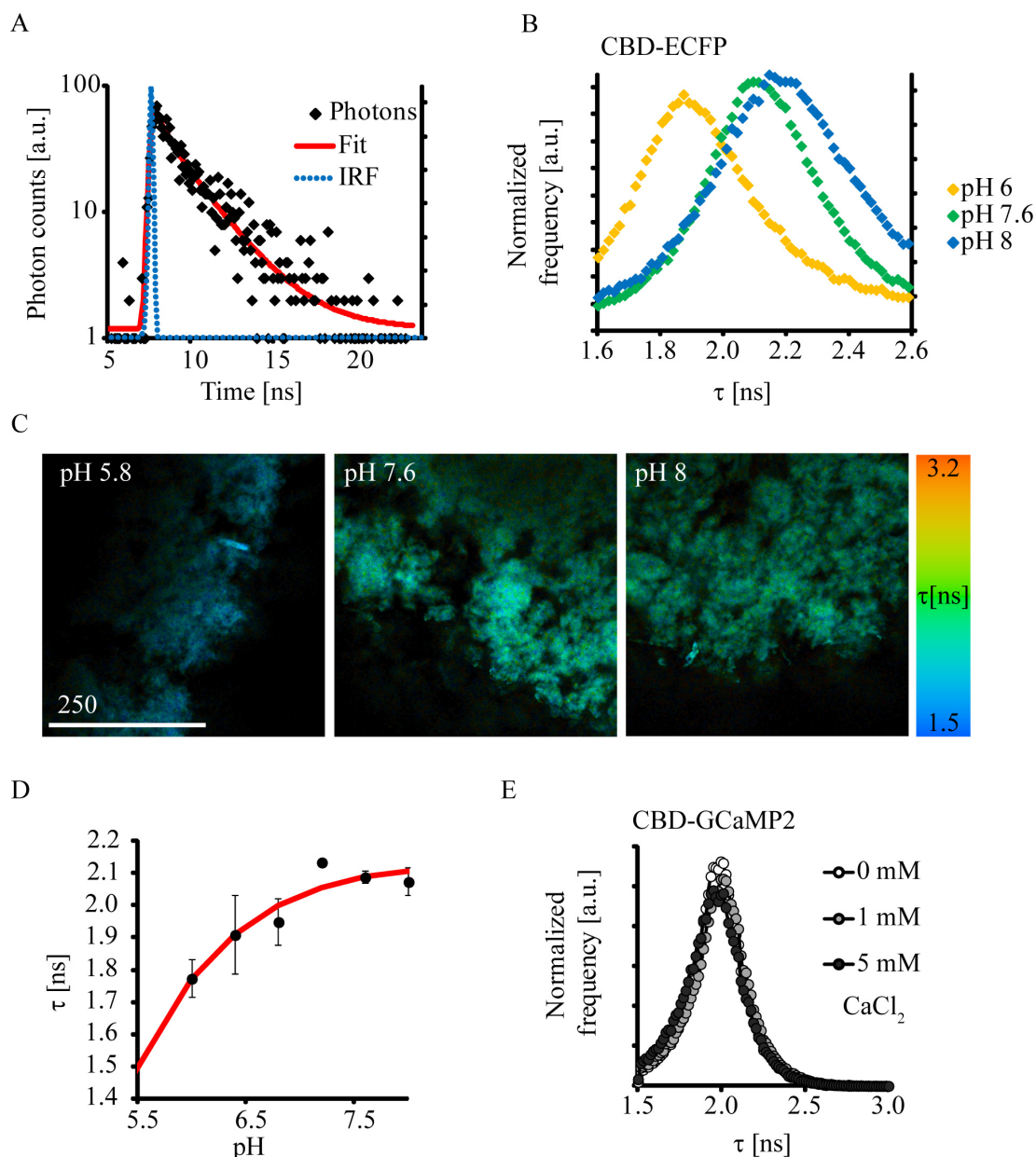


Figure 3. Evaluation of CBD-tagged biosensing scaffolds in FLIM. A: Example of fluorescence decay of CBD-ECFP bound GrowDex matrix (exc. 447 nm, em. 512-536 nm, pH 5.8). B: Fluorescence lifetime distributions (normalized by area) for CBD-ECFP GrowDex matrix exposed to different pH (37 °C). C: Fluorescence lifetime images for CBD-ECFP GrowDex matrix at different pH. Scale bar is in μm . D: pH FLIM calibration of CBD-ECFP, N=3. E: Fluorescence lifetime distributions for CBD-GCaMP2 labeled GrowDex at different CaCl₂ concentrations (exc. 488 nm, em. 512-536 nm).

3.3. Monitoring extracellular acidification in 3D culture of cancer cells

CBD-ECFP-stained cellulose scaffolds displayed no changes in structure (Fig. S5) and were subsequently tested for the ability to support cell growth. With stained and unstained GrowDex matrices and the culture of human colon cancer HCT116 cells we observed comparable cell growth over 3-7 days period in a Growdex matrix (Figure

S7). Interestingly, cells tended to form spheroid aggregates starting from day 2-3 and drastically reduced the numbers of single cells by day 7 (Figure S7).

In order to minimize shaking and vibration of scaffolds during the imaging procedure, we additionally embedded them in collagen-rich Matrigel matrix. Note that in addition to supporting function, Matrigel promotes growth and survival of cancer cell aggregates. Similar numbers and efficient 3D distribution of small cell aggregates (stained with the marker of mitochondria, TMRM) were evident (Fig. 4A-B). Notably, the CBD-ECFP-labeled GrowDex was distributed in patches across the volume of Matrigel matrix, which did not show any non-specific staining. We also tested bacterial cellulose and found that the cells grew within this matrix with significantly lower efficiency, probably due to lower porosity of produced matrices (not shown).

Next, we evaluated how the HCT116 cells (wild-type and oxidative phosphorylation-deficient knock-out cell line $\text{SCO}_2^{-/-}$) [69] can be studied by CBD-ECFP scaffolds in FLIM method. Fig. 4C shows examples of intensity images of cells (labeled with TMRM) and green fluorescent scaffold (intensity) as well as combined with FLIM images, produced from CBD-ECFP-labeled scaffold. Such co-localization allows identifying regions of cell culture, which are in contact with the scaffold. When we compared the average fluorescence lifetimes observed with wild-type and $\text{SCO}_2^{-/-}$ cultures, we found very similar pH values of 7.6-8, demonstrating no acidification of medium surrounding them (Fig. 4D). However, when we treated $\text{SCO}_2^{-/-}$ culture with mitochondrial uncoupler FCCP, we detected minor decrease of extracellular pH on distribution histograms, not seen with mock treatment (DMSO, Fig. 4EF). Despite the high variability and low sensitivity of ECFP protein in this pH range, we were able to identify statistically significant decrease in fluorescence lifetimes and pH for FCCP-treated samples (Fig. 4G). Since we had moderate density of cell population in produced scaffolds and the cell numbers per measured areas were variable, we could not see the higher magnitude of responses in extracellular acidification. Indeed, when we seeded HCT116 cells on a microplate at higher densities (10,000-100,000 cells per 0.32 cm^2 area) and measured their extracellular acidification we found drastic cell density-dependent changes, with much lower variability (Fig. S8). This shows that the sensitivity of single cell-based microscopy measurements can be improved with higher cell densities or larger size of aggregates.

Collectively, we demonstrated that CBD-ECFP-modified GrowDex scaffolds are compatible with cancer cell growth and subsequent analysis with FLIM method. While our microscope configuration did not allow for use of multiple fluorescent stains, it is clear that pH-FLIM performed for analysis of extracellular acidification can be multiplexed with other dyes, cell stains or even antibodies. We were not able to produce high cell densities in bacterial cellulose scaffold but GrowDex matrix allowed for efficient formation of small cell aggregates with no visible negative effects on cell growth.

Please cite this article as:

O'Donnell N, Okkelman IA, Timashev P, Gromovskiy TI, Papkovsky DB, Dmitriev RI: **Cellulose-based scaffolds for fluorescence lifetime imaging-assisted tissue engineering**. *Acta Biomaterialia* 2018, **80**:85-96.

Final manuscript version is available at:

<https://www.sciencedirect.com/science/article/pii/S1742706118305634>

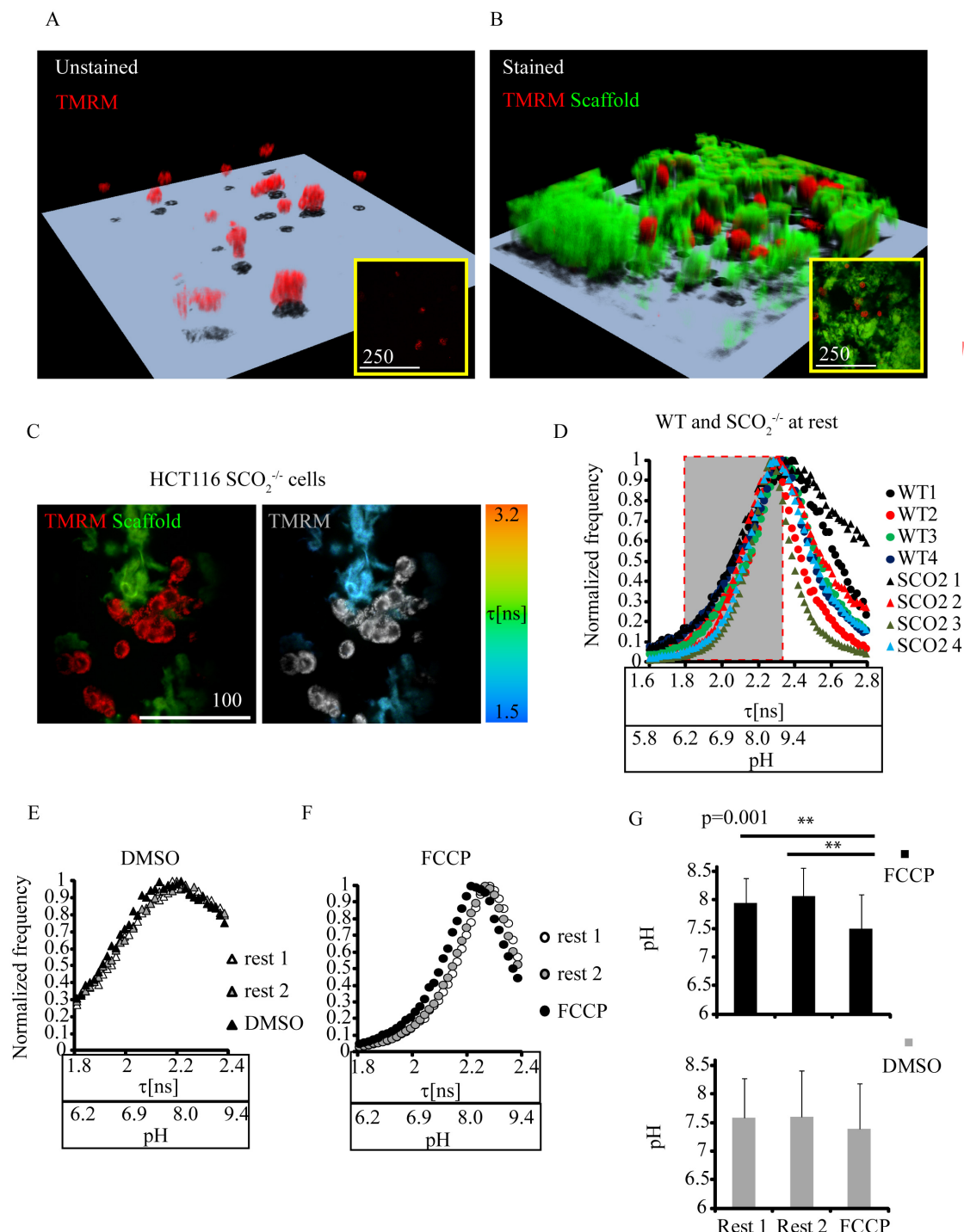


Figure 4. Sensing extracellular pH in CBD-ECFP GrowDex scaffolds populated with HCT116 cells. A, B: 3D reconstructions (76 μm thick Z stacks) of GrowDex scaffolds embedded in Matrigel, without and with staining with CBD-ECFP protein (green) and with growing HCT116 cells (red). C: Example of optical section with HCT116 $\text{SCO}_2^{-/-}$ cells growing within CBD-ECFP scaffold and showing co-localization in intensity images (green, red) and FLIM images (color scale, grayscale). D: Fluorescence lifetime distribution histograms (normalized by height) for resting wild-type and $\text{SCO}_2^{-/-}$ HCT116 cells. N=4. Scale bar is in μm . E, F, G: measured fluorescence lifetime distribution histograms for $\text{SCO}_2^{-/-}$

cells treated with DMSO and FCCP (E,F) and average pH values calculated during these stimulations. Statistically significant differences between means are indicated. N=3.

3.4. Plant-derived pH-sensitive scaffolds for multiplexed FLIM-PLIM microscopy of intestinal organoids

Recently introduced decellularized (DC) plant materials hold promise for advanced tissue engineering applications: they are cost-effective, widely available, come in variety of 3D architectures and are compatible with production of vascularized tissue constructs.

We thus evaluated in-house produced pH-sensitive DC spinach and celery scaffolds for 3D culture (section 3.2, Fig. S5-S6). We chose DC celery stems as they have high porosity and efficiency of specific staining with CBD-ECFP, probably due to more efficient mass exchange processes than in DC spinach (Fig. S5). The large vessels in DC celery stem can be also beneficial for uniform size distribution of cell aggregates. To test the feasibility of DC celery scaffolds modified with CBD-ECFP, we chose mouse intestinal organoids, produced from adult stem cells [53], for which we previously studied oxidative metabolism [65]. In order to grow organoids in the presence of native extracellular matrix, we seeded small intestinal crypts in DC celery together with Matrigel and grown them for 3-10 days. Prior to the measurements, organoids and DC celery scaffold were stained with CBD-ECFP and high-performance phosphorescent O₂-sensitive probe Pt-Glc [54].

With this setup we observed growth of organoids and efficient staining with pH and O₂ sensing materials, thus allowing combined FLIM and PLIM measurements. Fig. 5A shows examples of organoids (stained with red Pt-Glc probe) grown in DC celery scaffold (green fluorescence). Interestingly, using FLIM method and by simple separation of the fluorescence lifetimes, we could also distinguish the scaffold from the unstained organoid autofluorescence (indicated by yellow dashed line, Fig. 5B). Having both scaffold and organoids labeled with biosensors, we performed FLIM (to measure pH of scaffold material) combined with PLIM (to measure oxygenation of organoids), as shown with resting organoid in Fig. 5C. The strong autofluorescence of lumen shows different lifetimes in both PLIM (blue regions < 10 μ s) and FLIM (green-orange regions > 2 ns) images. Since the autofluorescence lifetime can potentially overlap with range of fluorescence lifetimes of CBD-ECFP, the images have to be analyzed for spatial localization of the objects, e.g. by using segmentation. When measured in the same sample, both Pt-Glc (PLIM) and CBD-ECFP, showed expected phosphorescence and fluorescence decay times and their distributions (Fig. 5DE).

Next, we tested how the combination of O₂ imaging using PLIM and pH imaging using FLIM can be used for studying dynamics of live organoid oxygenation and extracellular acidification, respectively. Fig. 5F shows example of superimposed images of organoid within the scaffold cavity as well as the separate FLIM and PLIM images. For the indicated region of contact between organoid and scaffold, we analyzed dynamics of pH and O₂ at rest and upon stimulations with mock (DMSO) and FCCP (Fig. 5G). We found that at rest the organoid already displayed strong deoxygenation (20-25 μ M instead of 40-80 μ M observed for conventional Matrigel culture [65]) and low extracellular pH (pH 6-6.2), presumably due to its high metabolic activity and static growth conditions. After stimulation we observed even

Please cite this article as:

O'Donnell N, Okkelman IA, Timashev P, Gromovych TI, Papkovsky DB, Dmitriev RI: **Cellulose-based scaffolds for fluorescence lifetime imaging-assisted tissue engineering**. *Acta Biomaterialia* 2018, **80**:85-96.

Final manuscript version is available at:

<https://www.sciencedirect.com/science/article/pii/S1742706118305634>

further decrease of pH, due to uncoupling of mitochondria with FCCP but no further specific decrease in oxygenation, possibly due to already hypoxic state of the organoid. This data confirms that organoids grown in DC celery scaffold remain viable and metabolically active. In addition, CBD-ECFP-labeled scaffolds can be efficiently used for combined monitoring of extracellular pH and cellular O₂ with organoid and potentially related 3D models.

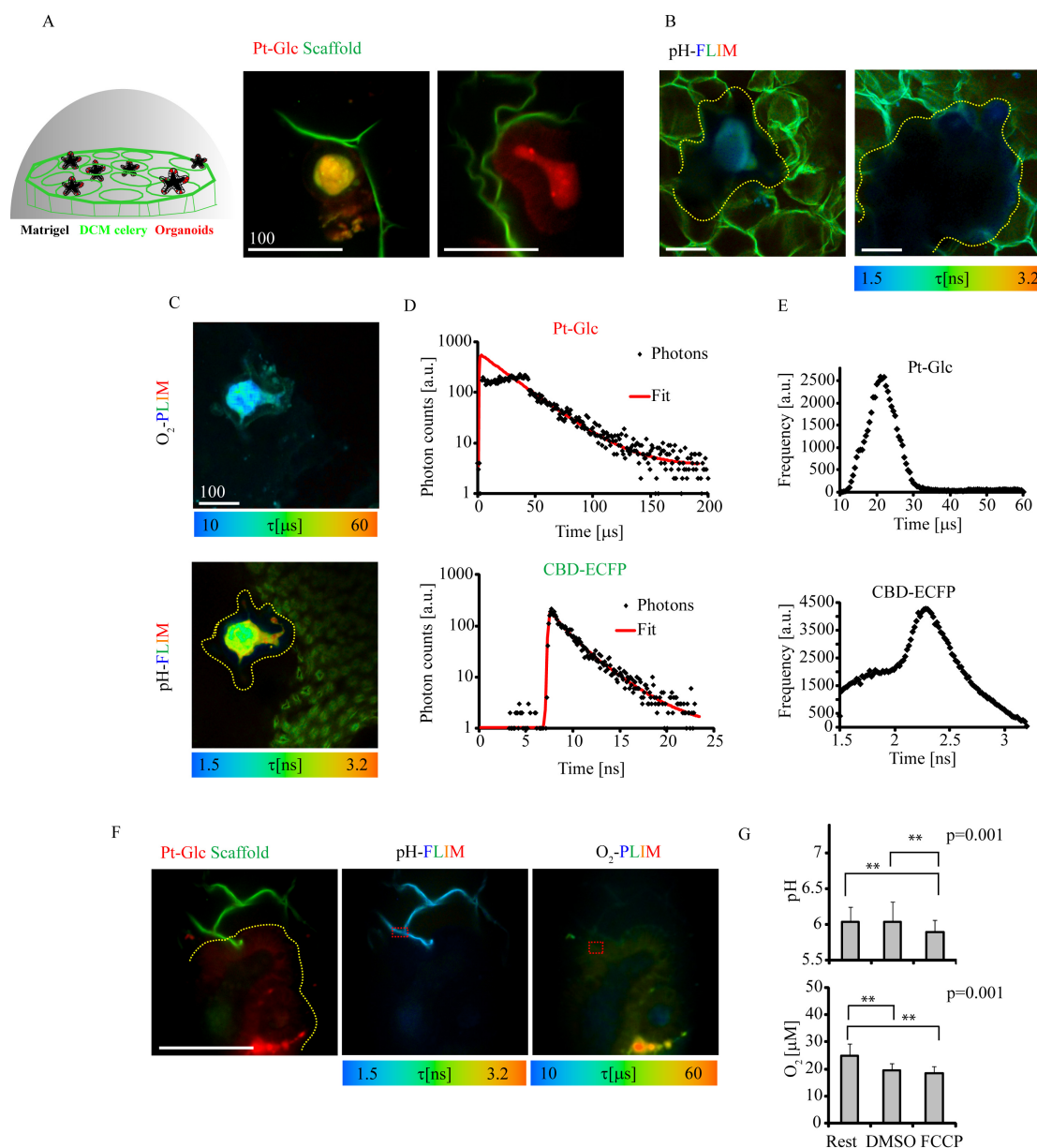


Figure 5. Sensing extracellular pH of intestinal organoids using CBD-ECFP in plant-derived scaffold model. A: examples of the intestinal organoids grown in scaffold stained with Pt-Glc (2 μM, 1 h, red, organoids) and CBD-ECFP (5 μM, 16 h, green, scaffold). B: examples of FLIM images of CBD-ECFP-stained DC celery with organoids (indicated by yellow dashed line). C: FLIM and PLIM images for the same organoid grown in vicinity of scaffold. D, E: characteristic luminescence lifetime decay fits (D) and distribution histograms

Please cite this article as:

O'Donnell N, Okkelman IA, Timashev P, Gromovych TI, Papkovsky DB, Dmitriev RI: **Cellulose-based scaffolds for fluorescence lifetime imaging-assisted tissue engineering**. *Acta Biomaterialia* 2018, **80**:85-96.

Final manuscript version is available at:

<https://www.sciencedirect.com/science/article/pii/S1742706118305634>

for PLIM and FLIM images shown in C. F: Combined intensity, FLIM (CBD-ECFP) and PLIM (Pt-Glc) images for selected organoid at rest. G: analysis of mean pH for selected regions of interest (F, selected regions are indicated by red dashed line) at rest and upon stimulation with 2 μ M FCCP. N=3. Asterisks indicate statistically significant differences. Scale bar is 100 μ m.

4. Conclusions

Here, we demonstrated design of biosensing scaffold-based materials for 3D cell culture, using genetic fusion of cellulose-binding domain with fluorescent protein. The variety and growing list of cellulose-based scaffold matrices especially produced by bio-printing or by direct decellularization of plants, provides a scope for the use of cellulose-binding domain (or related cellulose-binding polypeptides) in generating hybrid biosensing or other functional (e.g. photoactivated FRET biosensors) recombinant fluorescent protein-based materials. Two features make the described materials a perfect choice for designing similar and advanced sensors: (1) high specificity and broad variety of CBD and other carbohydrate-binding module sequences, and (2) growing toolbox of fluorescent proteins suitable for FLIM applications.

We found that fusing with CBD does not affect the fluorescence or biosensing properties of tested fluorescent proteins, ECFP and GCaMP2. Although GCaMP2 did not show sensing properties in fluorescence lifetime domain, a number of alternative biosensors can be considered, e.g. TN-XL or other proteins [37-39]. The performance of pH FLIM can be also significantly improved, e.g. by using superfolder YFP [10] or some newly developed proteins. While potentially the measurements of pH and Ca^{2+} can be performed in the intensity domain (using calculation of F/F_0), the fluorescence lifetime-based sensing is more robust with potential of 'once-off' calibration [27].

In contrast to the small molecule pH-sensitive dyes, which can be coupled covalently to the cellulose and related scaffolds, recombinant proteins promise higher biocompatibility, brightness, flexibility and potential for tuning of the number of bound proteins to the scaffold, e.g. by using CBD with various affinities towards the cellulose.

We successfully evaluated the pH-sensitive CBD-ECFP-labeled scaffolds, based on commercially available nanofibrillar cellulose (GrowDex) and decellularized plant materials (DC celery), with two different types of 3D tissue models: aggregates of human colon cancer cells HCT116 and adult stem cell-derived organoids. With both models we were able to detect pH-sensitive responses and no negative effects of the labeling of scaffold on the tissue viability or physiological status. Use of FLIM promises multiplexing options of CBD-ECFP-based pH sensing with a number of dyes and labels in intensity (e.g. with TMRM and related red mitochondrial stains) and with μ s-time domain (PLIM), for measuring oxygenation in a real-time. Thus, designed materials already allow for dual 'extracellular pH plus intracellular O_2 ' assays in 3D culture. They can be beneficial for assessing mitochondrial function, glycolysis, redox status and overall balance of energy production mechanisms, which can change during cell proliferation and differentiation or upon drug treatment, in stem and cancer cell cultures. Altogether, described approach opens new direction in design of bio-inspired sensing materials for quantitative microscopy of 3D cell models and organoids.

Please cite this article as:

O'Donnell N, Okkelman IA, Timashev P, Gromovych TI, Papkovsky DB, Dmitriev RI: **Cellulose-based scaffolds for fluorescence lifetime imaging-assisted tissue engineering**. *Acta Biomaterialia* 2018, **80**:85-96.

Final manuscript version is available at:

<https://www.sciencedirect.com/science/article/pii/S1742706118305634>

Supporting information

The Supporting information contains nucleotide and protein structures of the designed proteins, oligonucleotide primer sequences used in cloning and Supplementary figures S1-S8.

Acknowledgments:

This work was supported by Science Foundation Ireland (SFI) grants 13/SIRG/2144, 12/RC/2276 and Russian Science Foundation (RSF) grant 18-15-00407 (production of bacterial cellulose) and the Russian academic excellence project '5-100'. We are grateful to Dr. S.M. Borisov (Graz University of Technology) for assistance with solution-based fluorescence lifetime measurements, Dr. A. Jelzow (Becker & Hickl GmbH) for loan of 447 nm BDL-SMT laser, Dr. G. De Luca (SVI Huygens) for help with the data analysis, T. Foley (Dept. of Anatomy and Neuroscience), S. Ruane and C. Daly (School of Biochemistry) for technical assistance.

Competing interests statement

The authors do not have any competing interests.

Data availability statement

The raw / unprocessed data required to reproduce these findings cannot be shared this time due to technical or time limitations. However, they are freely available upon request.

References

- [1] A.P.C. Almeida, J.P. Canejo, S.N. Fernandes, C. Echeverria, P.L. Almeida, M.H. Godinho, Cellulose-Based Biomimetics and Their Applications, *Advanced Materials* (2018) 1703655.
- [2] D. Diekjürgen, D.W. Grainger, Polysaccharide matrices used in 3D in vitro cell culture systems, *Biomaterials* 141 (2017) 96-115.
- [3] P.B. Malafaya, G.A. Silva, R.L. Reis, Natural-origin polymers as carriers and scaffolds for biomolecules and cell delivery in tissue engineering applications, *Advanced drug delivery reviews* 59(4) (2007) 207-233.
- [4] T. Abitbol, A. Rivkin, Y. Cao, Y. Nevo, E. Abraham, T. Ben-Shalom, S. Lapidot, O. Shoseyov, Nanocellulose, a tiny fiber with huge applications, *Current Opinion in Biotechnology* 39 (2016) 76-88.
- [5] C.C. Piras, S. Fernández-Prieto, W.M. De Borggraeve, Nanocellulosic materials as bioinks for 3D bioprinting, *Biomaterials science* 5(10) (2017) 1988-1992.
- [6] A. Svensson, E. Nicklasson, T. Harrah, B. Panilaitis, D. Kaplan, M. Brittberg, P. Gatenholm, Bacterial cellulose as a potential scaffold for tissue engineering of cartilage, *Biomaterials* 26(4) (2005) 419-431.
- [7] C. Demitri, M.G. Raucci, A. Giuri, V.M. De Benedictis, D. Giugliano, P. Calcagnile, A. Sannino, L. Ambrosio, Cellulose-based porous scaffold for bone tissue engineering applications: Assessment of hMSC proliferation and differentiation, *Journal of Biomedical Materials Research Part A* 104(3) (2016) 726-733.
- [8] G. Feil, R. Horres, J. Schulte, A.F. Mack, S. Petzoldt, C. Arnold, C. Meng, L. Jost, J. Boxleitner, N. Kiessling-Wolf, Bacterial cellulose shifts transcriptome and proteome of cultured endothelial cells towards native differentiation, *Molecular & Cellular Proteomics* 16(9) (2017) 1563-1577.

Please cite this article as:

O'Donnell N, Okkelman IA, Timashev P, Gromovych TI, Papkovsky DB, Dmitriev RI: **Cellulose-based scaffolds for fluorescence lifetime imaging-assisted tissue engineering**. *Acta Biomaterialia* 2018, **80**:85-96.

Final manuscript version is available at:

<https://www.sciencedirect.com/science/article/pii/S1742706118305634>

- [9] Z. Di, Z. Shi, M.W. Ullah, S. Li, G. Yang, A transparent wound dressing based on bacterial cellulose whisker and poly (2-hydroxyethyl methacrylate), *International journal of biological macromolecules* 105 (2017) 638-644.
- [10] T. Consolati, J.M. Bolivar, Z. Petrasek, J. Berenguer, A. Hidalgo, J.M. Guisán, B. Nidetzky, Bio-based, internally pH sensitive materials: immobilized yellow fluorescent protein as optical sensor for spatiotemporal mapping of pH inside porous matrices, *ACS applied materials & interfaces* 10(8) (2018) 6858-6868.
- [11] W. Thongsomboon, D.O. Serra, A. Possling, C. Hadjineophytou, R. Hengge, L. Cegelski, Phosphoethanolamine cellulose: A naturally produced chemically modified cellulose, *Science* 359(6373) (2018) 334-338.
- [12] J.R. Gershlak, S. Hernandez, G. Fontana, L.R. Perreault, K.J. Hansen, S.A. Larson, B.Y. Binder, D.M. Dolivo, T. Yang, T. Dominko, Crossing kingdoms: Using decellularized plants as perfusable tissue engineering scaffolds, *Biomaterials* 125 (2017) 13-22.
- [13] G. Fontana, J. Gershlak, M. Adamski, J.S. Lee, S. Matsumoto, H.D. Le, B. Binder, J. Wirth, G. Gaudette, W.L. Murphy, Biofunctionalized Plants as Diverse Biomaterials for Human Cell Culture, *Advanced Healthcare Materials* 6(8) (2017).
- [14] Y. Wang, R. Kim, D.B. Gunasekara, M.I. Reed, M. DiSalvo, D.L. Nguyen, S.J. Bultman, C.E. Sims, S.T. Magness, N.L. Allbritton, Formation of human colonic crypt array by application of chemical gradients across a shaped epithelial monolayer, *Cellular and Molecular Gastroenterology and Hepatology* 5(2) (2018) 113-130.
- [15] A.A. Appel, M.A. Anastasio, J.C. Larson, E.M. Brey, Imaging challenges in biomaterials and tissue engineering, *Biomaterials* 34(28) (2013) 6615-6630.
- [16] L. Teodori, A. Crupi, A. Costa, A. Diaspro, S. Melzer, A. Tarnok, Three-dimensional imaging technologies: a priority for the advancement of tissue engineering and a challenge for the imaging community, *Journal of biophotonics* 10(1) (2017) 24-45.
- [17] S.W. Lane, D.A. Williams, F.M. Watt, Modulating the stem cell niche for tissue regeneration, *Nature biotechnology* 32(8) (2014) 795.
- [18] D.W. Hutmacher, R.E. Horch, D. Loessner, S. Rizzi, S. Sieh, J.C. Reichert, J.A. Clements, J.P. Beier, A. Arkudas, O. Bleiziffer, Translating tissue engineering technology platforms into cancer research, *Journal of cellular and molecular medicine* 13(8a) (2009) 1417-1427.
- [19] D.A. Ferrick, A. Neilson, C. Beeson, Advances in measuring cellular bioenergetics using extracellular flux, *Drug discovery today* 13(5) (2008) 268-274.
- [20] A. Zhdanov, C. Favre, L. O'Flaherty, J. Adam, R. O'Connor, P. Pollard, D. Papkovsky, Comparative bioenergetic assessment of transformed cells using a cell energy budget platform, *Integrative Biology* 3(11) (2011) 1135-1142.
- [21] K.K. Kaysinger, W.K. Ramp, Extracellular pH modulates the activity of cultured human osteoblasts, *Journal of cellular biochemistry* 68(1) (1998) 83-89.
- [22] K. Lee, E.A. Silva, D.J. Mooney, Growth factor delivery-based tissue engineering: general approaches and a review of recent developments, *Journal of the Royal Society Interface* 8(55) (2011) 153-170.
- [23] M.H. Wu, J.P. Urban, Z.F. Cui, Z. Cui, X. Xu, Effect of extracellular pH on matrix synthesis by chondrocytes in 3D agarose gel, *Biotechnology progress* 23(2) (2007) 430-434.
- [24] E.M. Brown, R.J. MacLeod, Extracellular calcium sensing and extracellular calcium signaling, *Physiological reviews* 81(1) (2001) 239-297.
- [25] A.V. Zhdanov, M.W. Ward, C.T. Taylor, E.A. Souslova, D.M. Chudakov, J.H.M. Prehn, D.B. Papkovsky, Extracellular calcium depletion transiently elevates oxygen consumption in neurosecretory PC12 cells through activation of mitochondrial Na⁺/Ca²⁺ exchange, *Biochimica et Biophysica Acta (BBA) - Bioenergetics* 1797(9) (2010) 1627-1637.

Please cite this article as:

O'Donnell N, Okkelman IA, Timashev P, Gromovskiy TI, Papkovsky DB, Dmitriev RI: **Cellulose-based scaffolds for fluorescence lifetime imaging-assisted tissue engineering**. *Acta Biomaterialia* 2018, **80**:85-96.

Final manuscript version is available at:

<https://www.sciencedirect.com/science/article/pii/S1742706118305634>

- [26] N. O'Donnell, R.I. Dmitriev, Three-Dimensional Tissue Models and Available Probes for Multi-Parametric Live Cell Microscopy: A Brief Overview, *Multi-Parametric Live Cell Microscopy of 3D Tissue Models*, Springer 2017, pp. 49-67.
- [27] P. Sarder, D. Maji, S. Achilefu, Molecular probes for fluorescence lifetime imaging, *Bioconjugate chemistry* 26(6) (2015) 963-974.
- [28] K. Suhling, L.M. Hirvonen, J.A. Levitt, P.-H. Chung, C. Tregidgo, A. Le Marois, D.A. Rusakov, K. Zheng, S. Ameer-Beg, S. Poland, Fluorescence lifetime imaging (FLIM): Basic concepts and some recent developments, *Medical Photonics* 27 (2015) 3-40.
- [29] A. Le Marois, K. Suhling, Quantitative Live Cell FLIM Imaging in Three Dimensions, *Multi-Parametric Live Cell Microscopy of 3D Tissue Models*, Springer 2017, pp. 31-48.
- [30] D.B. Papkovsky, R.I. Dmitriev, Imaging of oxygen and hypoxia in cell and tissue samples, *Cellular and Molecular Life Sciences* (2018).
- [31] S. Poëa-Guyon, H. Pasquier, F. Mérola, N. Morel, M. Erard, The enhanced cyan fluorescent protein: a sensitive pH sensor for fluorescence lifetime imaging, *Analytical and bioanalytical chemistry* 405(12) (2013) 3983-3987.
- [32] M. Tantama, Y.P. Hung, G. Yellen, Imaging intracellular pH in live cells with a genetically encoded red fluorescent protein sensor, *Journal of the American Chemical Society* 133(26) (2011) 10034-10037.
- [33] H.J. Lin, P. Herman, J.R. Lakowicz, Fluorescence lifetime-resolved pH imaging of living cells, *Cytometry Part A* 52(2) (2003) 77-89.
- [34] C. Hille, M. Berg, L. Bressel, D. Munzke, P. Primus, H.-G. Löhmannsröben, C. Dosche, Time-domain fluorescence lifetime imaging for intracellular pH sensing in living tissues, *Analytical and bioanalytical chemistry* 391(5) (2008) 1871.
- [35] D. Aigner, R. Dmitriev, S. Borisov, D. Papkovsky, I. Klimant, pH-sensitive perylene bisimide probes for live cell fluorescence lifetime imaging, *Journal of Materials Chemistry B* 2(39) (2014) 6792-6801.
- [36] T. Gensch, D. Kaschuba, Fluorescent genetically encoded calcium indicators and their in vivo application, *Fluorescent Proteins II*, Springer 2011, pp. 125-161.
- [37] B. Sauer, Q. Tian, P. Lipp, L. Kaestner, Confocal FLIM of genetically encoded FRET sensors for quantitative Ca²⁺ imaging, *Cold Spring Harbor Protocols* 2014(12) (2014) pdb. prot077040.
- [38] J.L. Rinnenthal, C. Börnchen, H. Radbruch, V. Andresen, A. Mossakowski, V. Siffrin, T. Seelemann, H. Spiecker, I. Moll, J. Herz, Parallelized TCSPC for dynamic intravital fluorescence lifetime imaging: quantifying neuronal dysfunction in neuroinflammation, *PLoS One* 8(4) (2013) e60100.
- [39] M. Mank, D.F. Reiff, N. Heim, M.W. Friedrich, A. Borst, O. Griesbeck, A FRET-based calcium biosensor with fast signal kinetics and high fluorescence change, *Biophysical journal* 90(5) (2006) 1790-1796.
- [40] K. Presley, J. Hwang, S. Cheong, R. Tilley, J. Collins, M. Viapiano, J. Lannutti, Nanoscale upconversion for oxygen sensing, *Materials Science and Engineering: C* 70 (2017) 76-84.
- [41] G. Yazgan, R.I. Dmitriev, V. Tyagi, J. Jenkins, G.-M. Rotaru, M. Rottmar, R.M. Rossi, C. Toncelli, D.B. Papkovsky, K. Maniura-Weber, Steering surface topographies of electrospun fibers: understanding the mechanisms, *Scientific Reports* 7 (2017).
- [42] J. Jenkins, R.I. Dmitriev, K. Morten, K.W. McDermott, D.B. Papkovsky, Oxygen-sensing scaffolds for 3-dimensional cell and tissue culture, *Acta Biomaterialia* 16 (2015) 126-135.
- [43] B. Schyrr, S. Pasche, G. Voirin, C. Weder, Y.C. Simon, E.J. Foster, Biosensors Based on Porous Cellulose Nanocrystal-Poly(vinyl Alcohol) Scaffolds, *ACS Applied Materials & Interfaces* 6(15) (2014) 12674-12683.

Please cite this article as:

O'Donnell N, Okkelman IA, Timashev P, Gromovskiy TI, Papkovsky DB, Dmitriev RI: **Cellulose-based scaffolds for fluorescence lifetime imaging-assisted tissue engineering**. *Acta Biomaterialia* 2018, **80**:85-96.

Final manuscript version is available at:

<https://www.sciencedirect.com/science/article/pii/S1742706118305634>

- [44] A. Almeida, A.M.M. Rosa, A.M. Azevedo, D.M.F. Prazeres, A biomolecular recognition approach for the functionalization of cellulose with gold nanoparticles, *Journal of Molecular Recognition* 30(9) (2017) e2634.
- [45] X. Meng, K.J. Edgar, "Click" reactions in polysaccharide modification, *Progress in Polymer Science* 53 (2016) 52-85.
- [46] J.R.G. Navarro, G. Conzatti, Y. Yu, A.B. Fall, R. Mathew, M. Edén, L. Bergström, Multicolor Fluorescent Labeling of Cellulose Nanofibrils by Click Chemistry, *Biomacromolecules* 16(4) (2015) 1293-1300.
- [47] J.R.G. Navarro, S. Wennmalm, J. Godfrey, M. Breitholtz, U. Edlund, Luminescent Nanocellulose Platform: From Controlled Graft Block Copolymerization to Biomarker Sensing, *Biomacromolecules* 17(3) (2016) 1101-1109.
- [48] C. Oliveira, V. Carvalho, L. Domingues, F.M. Gama, Recombinant CBM-fusion technology—applications overview, *Biotechnology advances* 33(3) (2015) 358-369.
- [49] K. Terpe, Overview of tag protein fusions: from molecular and biochemical fundamentals to commercial systems, *Applied microbiology and biotechnology* 60(5) (2003) 523-533.
- [50] P. Tomme, A. Boraston, B. McLean, J. Kormos, A.L. Creagh, K. Sturch, N.R. Gilkes, C.A. Haynes, R.A.J. Warren, D.G. Kilburn, Characterization and affinity applications of cellulose-binding domains, *Journal of Chromatography B: Biomedical Sciences and Applications* 715(1) (1998) 283-296.
- [51] N. Din, I.J. Forsythe, L.D. Burtnick, N.R. Gilkes, R.C. Miller, R.A.J. Warren, D.G. Kilburn, The cellulose-binding domain of endoglucanase A (CenA) from *Cellulomonas fimi*: evidence for the involvement of tryptophan residues in binding, *Molecular microbiology* 11(4) (1994) 747-755.
- [52] Q. Wang, B. Shui, M.I. Kotlikoff, H. Sondermann, Structural Basis for Calcium Sensing by GCaMP2, *Structure* 16(12) (2008) 1817-1827.
- [53] I.A. Okkelman, T. Foley, D.B. Papkovsky, R.I. Dmitriev, Multi-Parametric Imaging of Hypoxia and Cell Cycle in Intestinal Organoid Culture, in: R. Dmitriev (Ed.), *Multi-Parametric Live Cell Microscopy of 3D Tissue Models*, *Advances in Experimental Medicine and Biology*, Springer, Cham, 2017, pp. 85-103.
- [54] R.I. Dmitriev, A.V. Kondrashina, K. Koren, I. Klimant, A.V. Zhdanov, J.M. Pakan, K.W. McDermott, D.B. Papkovsky, Small molecule phosphorescent probes for O₂ imaging in 3D tissue models, *Biomaterials Science* 2(6) (2014) 853-866.
- [55] A.S. Rose, P.W. Hildebrand, NGL Viewer: a web application for molecular visualization, *Nucleic acids research* 43(W1) (2015) W576-W579.
- [56] J. Akerboom, J.D.V. Rivera, M.M.R. Guilbe, E.C.A. Malavé, H.H. Hernandez, L. Tian, S.A. Hires, J.S. Marvin, L.L. Looger, E.R. Schreier, Crystal structures of the GCaMP calcium sensor reveal the mechanism of fluorescence signal change and aid rational design, *Journal of biological chemistry* 284(10) (2009) 6455-6464.
- [57] M. Lelievre, M. Noirel-Savoye, C. Lazareno-Saez, B. Paetzold, S. Le Vot, R. Chazal, P. Macheboeuf, M.J. Field, D. Bourgeois, A. Royant, Intrinsic dynamics in ECFP and Cerulean control fluorescence quantum yield, *Biochemistry* 48(42) (2009) 10038-10046.
- [58] G.-Y. Xu, E. Ong, N.R. Gilkes, D.G. Kilburn, D. Muhandiram, M. Harris-Brandts, J.P. Carver, L.E. Kay, T.S. Harvey, Solution structure of a cellulose-binding domain from *Cellulomonas fimi* by nuclear magnetic resonance spectroscopy, *Biochemistry* 34(21) (1995) 6993-7009.
- [59] S. Hestrin, M. Schramm, Synthesis of cellulose by *Acetobacter xylinum*. 2. Preparation of freeze-dried cells capable of polymerizing glucose to cellulose, *Biochemical Journal* 58(2) (1954) 345.

Please cite this article as:

O'Donnell N, Okkelman IA, Timashev P, Gromovych TI, Papkovsky DB, Dmitriev RI: **Cellulose-based scaffolds for fluorescence lifetime imaging-assisted tissue engineering**. *Acta Biomaterialia* 2018, **80**:85-96.

Final manuscript version is available at:

<https://www.sciencedirect.com/science/article/pii/S1742706118305634>

- [60] R.I. Dmitriev, A.V. Zhdanov, G. Jasione, D.B. Papkovsky, Assessment of cellular oxygen gradients with a panel of phosphorescent oxygen-sensitive probes, *Analytical chemistry* 84(6) (2012) 2930-2938.
- [61] R.I. Dmitriev, N. O'Donnell, D.B. Papkovsky, Metallochelat Coupling of Phosphorescent Pt-Porphyrins to Peptides, Proteins, and Self-Assembling Protein Nanoparticles, *Bioconjugate chemistry* 27(2) (2016) 439-445.
- [62] R.I. Dmitriev, S.M. Borisov, H. Dössmann, S. Sun, B.J. Müller, J. Prehn, V.P. Baklaushev, I. Klimant, D.B. Papkovsky, Versatile conjugated polymer nanoparticles for high-resolution O₂ imaging in cells and 3D tissue models, *ACS nano* 9(5) (2015) 5275-5288.
- [63] J. Jenkins, S.M. Borisov, D.B. Papkovsky, R.I. Dmitriev, Sulforhodamine nanothermometer for multiparametric fluorescence lifetime imaging microscopy, *Analytical chemistry* 88(21) (2016) 10566-10572.
- [64] I.A. Okkelman, R.I. Dmitriev, T. Foley, D.B. Papkovsky, Use of fluorescence lifetime imaging microscopy (FLIM) as a timer of cell cycle S phase, *PloS one* 11(12) (2016) e0167385.
- [65] I.A. Okkelman, T. Foley, D.B. Papkovsky, R.I. Dmitriev, Live cell imaging of mouse intestinal organoids reveals heterogeneity in their oxygenation, *Biomaterials* 146 (2017) 86-96.
- [66] P. Tomme, N.R. Gilkes, R.C. Miller Jr, A.J. Warren, D.G. Kilburn, An internal cellulose-binding domain mediates adsorption of an engineered bifunctional xylanase/cellulase, *Protein Engineering, Design and Selection* 7(1) (1994) 117-123.
- [67] Y.N. Tallini, M. Ohkura, B.-R. Choi, G. Ji, K. Imoto, R. Doran, J. Lee, P. Plan, J. Wilson, H.-B. Xin, Imaging cellular signals in the heart in vivo: Cardiac expression of the high-signal Ca²⁺ indicator GCaMP2, *Proceedings of the National Academy of Sciences of the United States of America* 103(12) (2006) 4753-4758.
- [68] J. Nakai, M. Ohkura, K. Imoto, A high signal-to-noise Ca²⁺ probe composed of a single green fluorescent protein, *Nature biotechnology* 19(2) (2001) 137-141.
- [69] H.J. Sung, W. Ma, P.-y. Wang, J. Hynes, T.C. O'riordan, C.A. Combs, J.P. McCoy Jr, F. Bunz, J.-G. Kang, P.M. Hwang, Mitochondrial respiration protects against oxygen-associated DNA damage, *Nature communications* 1 (2010) 5.